Journal of Geophysical Research: Atmospheres

RESEARCH ARTICLE
10.1002/2017JD027631

Key Points:
- EnSRF was used to assimilate $PM_{2.5}$ observations and source emissions during the 2015 China Victory Day parade emissions regulation period
- The spatial and temporal variation of the source emissions during different stages of regulation was reasonably estimated
- Sensitivity experiments further highlighted the valuable impact of different strategies for emissions regulations

Supporting Information:
- Supporting Information S1
- Data Set S1

Correspondence to:
Z. Peng,
pengzhen@nju.edu.cn

Citation:
Chu, K., Peng, Z., Liu, Z., Lei, L., Kou, X., Zhang, Y., Bo, X., & Tian, J. (2018). Evaluating the impact of emissions regulations on the emissions reduction during the 2015 China Victory Day parade with an ensemble square root filter. *Journal of Geophysical Research: Atmospheres*, *123*, 4122–4134. https://doi.org/10.1002/2017JD027631

Received 20 AUG 2017
Accepted 27 MAR 2018
Accepted article online 2 APR 2018
Published online 16 APR 2018

Evaluating the Impact of Emissions Regulations on the Emissions Reduction During the 2015 China Victory Day Parade With an Ensemble Square Root Filter

Kekuan Chu[1,2], Zhen Peng[2], Zhiquan Liu[3], Lili Lei[1,2], Xingxia Kou[4], Yi Zhang[1,2], Xin Bo[5], and Jun Tian[6]

[1]Key Laboratory of Mesoscale Severe Weather/Ministry of Education, Nanjing University, Nanjing, China, [2]School of Atmospheric Sciences, Nanjing University, Nanjing, China, [3]National Center for Atmospheric Research, Boulder, CO, USA, [4]Institute of Urban Meteorology, CMA, Beijing, China, [5]Appraisal Center for Environment and Engineering, MEP, Beijing, China, [6]Academy of Environmental Planning and Design, Co., Ltd, Nanjing University, Nanjing, China

Abstract In order to guarantee good air quality for the 15th International Association of Athletics Federations World Championships (22–30 August) and the China Victory Day parade (3 September) in Beijing, a series of comprehensive emissions regulations were implemented in Beijing and the surrounding provinces from 20 August to 3 September 2015. During this period, the intensity of the emissions regulation was enhanced step by step in the run-up to the event. This period therefore allowed us to quantitatively estimate the reduction in emissions as a result of the emissions regulations under different intensity and strategy scenarios. The ensemble square root filter was employed to optimize the initial conditions and the emissions simultaneously. Numerical results showed that the variations of the anthropogenic emissions before, during, and after the emissions regulations were reasonably simulated. The updated emissions were about 80% and 50% of the prior anthropogenic emissions during the regular- and stringent-regulations periods, respectively. As a result, the $PM_{2.5}$ concentrations consistently reduced during the regulations period, and the largest reduction occurred under the stringent-regulations period. Sensitivity simulations forced by the averaged emissions before the regulations and during the regular- and stringent-regulation periods further highlighted the valuable impacts of emissions regulations, under different strategy and intensity scenarios, on the improvement of air quality. More intense emissions regulation will lead to a greater reduction in $PM_{2.5}$ concentrations.

1. Introduction

During recent decades China has been suffering from severe air pollution, especially in urban areas with high population densities (Chan & Yao, 2008; Chen et al., 2014), which is a byproduct of rapid economic growth. Consistent efforts, such as the "Atmospheric Pollution Prevention and Control Action Plan," have been implemented by the government to control $PM_{2.5}$ (particulate matter with an aerodynamic diameter of 2.5 μm or less) pollution and to improve air quality. In addition to long-term air pollution control, temporary air pollution regulations have also occasionally been implemented to guarantee good air quality during major events, such as the 2008 Beijing Olympic Games (Okuda et al., 2011; Streets et al., 2007; Wang, Liang, et al., 2010; Wang, Nie, et al., 2010; Wang et al., 2014; Zhou et al., 2012) and the 2014 Asia-Pacific Economic Cooperation (APEC) Summit held in Beijing (Huang et al., 2015; Tang et al., 2015; Wen et al., 2016; Zhang et al., 2016). These temporary regulations resulted in the so-called "Olympic blue" and "APEC blue" in the years those events took place.

With the government and public paying increasing levels of attention to air pollution control, quantitatively evaluating the achievements in the air quality resulting from various regulation measures is imperative and valuable for government policy makers. First, it is vital to be able to estimate real-time emissions sources accurately. However, this is difficult because most emissions inventories are developed based on a bottom-up approach, which is dependent on land use, the source sector, and sector-specific emissions factors, which introduces considerable uncertainty in the data (Ding et al., 2015). Data assimilation approaches are frequently used to estimate or improve estimations of source emissions. Such efforts include variational approaches (Chai et al., 2007; Elbern et al., 2007; Guerrette & Henze, 2015; Hakami et al., 2005; Henze et al., 2007, 2009; Wang et al., 2012; Yumimoto et al., 2007, 2008; Zhang et al., 2016; Zhu et al., 2013) and ensemble-based approaches (Barbu et al.,

2009; Constantinescu et al., 2007a, 2007b; Heemink & Segers, 2002; Huneeus et al., 2012, 2013; Miyazaki et al., 2014; Schutgens et al., 2010; Sekiyama et al., 2010; Tang et al., 2011; Wang et al., 2016).

Accurately estimating source emissions is crucial for $PM_{2.5}$ prediction and can also provide timely instructions for the design of future emissions regulations. Tang et al. (2011) reported that simultaneously assimilating ozone (O_3), nitrogen oxide, and volatile organic compound observations and their emissions can result in better 1-hr and 24-hr O_3 forecasts than through the individual assimilation of concentrations or emissions. Miyazaki et al. (2012) also highlighted the importance of the simultaneous adjustment of concentrations and emissions for improving tropospheric O_3 budget and profile analyses. Recently, Peng et al. (2017) improved a $PM_{2.5}$ concentration forecast over China by simultaneously optimizing the chemical initial conditions and source emission inputs.

From 20 August to 3 September 2015, to guarantee good air quality for the 15th International Association of Athletics Federations World Championships (22–30 August) and the China Victory Day parade (3 September) in Beijing, a series of comprehensive emissions regulations were implemented in Beijing and surrounding provinces. These emissions regulations included two stages (Xue et al., 2017): regular regulation (20–31 August) and stringent regulation (1–3 September). From 20 August onward, Beijing and nearby provinces (Hebei, Shanxi, Shandong, Tianjin City, and the Inner Mongolia Autonomous Region) began to gradually implement emissions regulations. The emissions regulations focused on the control of heavy industry pollution, coal-burning pollution, transportation pollution, and fugitive dust pollution, with a main focus on reducing the emissions of sulfur dioxide (SO_2), nitrogen oxide, volatile organic compounds, and fugitive dust (Wen et al., 2016). Moreover, traffic restrictions based on even- and odd-numbered license plates were implemented for private vehicles, and at least 80% of the vehicles used by government bureaus and institutes, and all high-emitting vehicles (with yellow environmental labels), were banned from use. As the event approached, stringent regulations were enforced from 1 to 3 September, aimed at achieving an emissions reduction of at least 30% in both moderate- and high-impact regions. Polluting enterprises suspended production, and construction sites were temporarily closed. Through these comprehensive emissions regulations, the average $PM_{2.5}$ concentration in Beijing during the control period was down 73.1%, which was only 18 $\mu g/m^3$ (http://www.mep.gov.cn/gkml/hbb/qt/201509/t20150907_309462.htm, Ministry of Environmental Protection of the People's Republic of China). Furthermore, the $PM_{2.5}$ concentration of the adjacent provinces was also greatly reduced. Similar to "Olympic blue" and "APEC blue," the consistently blue skies during this period were named "parade blue."

Many studies have focused on this event (Lin et al., 2017; Liu et al., 2016; Zhao et al., 2017). Observations have shown that there was a decreasing trend in concentrations of water-soluble ions and aerosol sulfate (Han et al., 2016), as well as a consistent reduction in $PM_{2.5}$, PM_{10} (coarse particulate matter), nitrogen dioxide, SO_2, and carbon monoxide concentrations (Xu et al., 2017) in Beijing and its surrounding area during the emissions control period. Xue et al. (2017) concluded that the absolute reduction in emissions of primary air pollutants led to the reduced $PM_{2.5}$ concentration. Wang et al. (2017) further noted that local emissions reduction contributed more to the air quality in Beijing than that from neighboring regions of Beijing, and the meteorological conditions were also beneficial for the improvement in air quality. The above analyses were mostly based on observations of $PM_{2.5}$ and its components. However, an accurate estimation of spatial and temporal variations of the reductions in source emissions during this period has not yet been reported. During this period, the regulation measures were enhanced step by step, which provides us with a unique opportunity to quantitatively evaluate the impact of the regulation measures at different intensities on the reduction in source emissions and the subsequent improvements in air quality during the event. This was the primary goal of the present reported work.

Section 2 describes the emissions estimation method proposed by Peng et al. (2017), the observations used in the study, and the experimental design. The main numerical results are present in section 3. A summary and discussion are given in section 4.

2. Methods, Data and Experimental Design

2.1. Emissions Data Assimilation Approach

The emissions data assimilation approach employed was the same as in Peng et al. (2017). The forecasting model included two parts: the Weather Research and Forecasting (WRF)-Chem model (Grell et al., 2005),

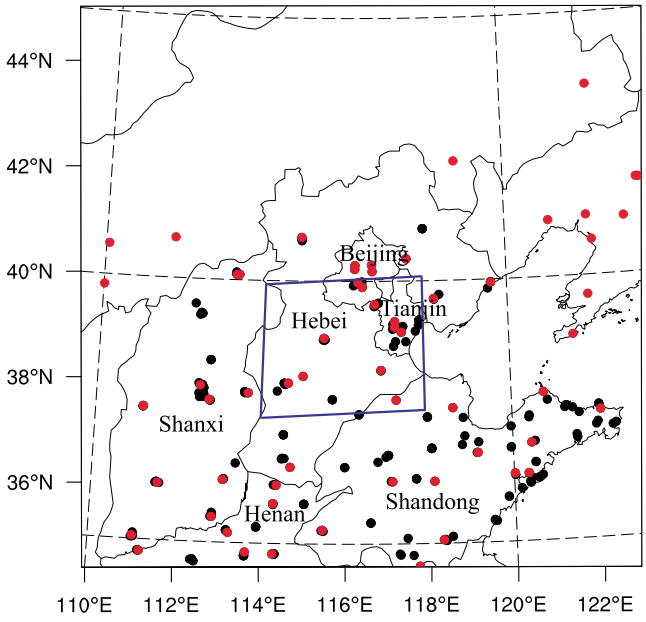

Figure 1. Locations of the 76 $PM_{2.5}$ assimilation observation stations (black dots) and 131 independent observation stations (red dots) in the model domain. The blue box marks the south Beijing-Tianjin-Hebei region.

which was used to predict the transport of aerosol and chemical species, and a persistence forecasting operator of emissions, which was added to forecast the background fields of the emissions scaling factors $\lambda^{f}_{i,t}$. This forecast operator was constructed by using the ensemble concentration ratios of the WRF-Chem forecast chemical concentrations and the time smoothing operator. Thus,

$$\kappa_{i,t} = \frac{\mathbf{c}^{f}_{i,t}}{\overline{\mathbf{c}^{f}_{t}}}, (i = 1, \ldots, N), \tag{1}$$

$$\left(\kappa_{i,t}\right)_{\inf} = \beta\left(\kappa_{i,t} - 1\right) + 1, (i = 1, \ldots, N), \tag{2}$$

$$\lambda^{p}_{i,t} = \left(\kappa_{i,t}\right)_{\inf}, (i = 1, \ldots, N), \tag{3}$$

$$\lambda^{f}_{i,t} = \frac{1}{M}\left(\sum_{j=t-M+1}^{t-1} \lambda^{a}_{i,j} + \lambda^{p}_{i,t}\right), (\, i = 1, \ldots, N, j = t - M + 1, \ldots, t - 1), \tag{4}$$

where $\mathbf{c}^{f}_{i,t}$ are the chemical fields at time t, which were available in the previous assimilation cycle via WRF-Chem; $\overline{\mathbf{c}^{f}_{t}} = \frac{1}{N}\sum_{i=1}^{N} \mathbf{c}^{f}_{i,t}$ is the ensemble mean of the chemical fields; $\kappa_{i,\,t}$ are the ensemble concentration scaling factors; β is the inflation factor to ensure the ensemble spread of the concentration scaling factors at a certain level, which was taken as 2.0; M is the time window of the time smoothing operator, chosen as 4 hr; and $\lambda^{a}_{i,j}\ (\, i = 1, \ldots, N, j = t - M + 1, \ldots, t - 1)$ are the previous data assimilation cycles' analysis scaling factors.

Then, the ensemble members of the forecast emissions, which were used to force the ensemble forecast for WRF-Chem, were calculated using the equation

$$\boldsymbol{E}^{f}_{i,t} = \lambda^{f}_{i,t}\boldsymbol{E}^{p}_{t}, (i = 1, \ldots, N), \tag{5}$$

where $\boldsymbol{E}^{f}_{i,t}$ is the ith ensemble member of the forecast emissions at time t, $\lambda^{f}_{i,t}$ is the forecast scaling factors, and $\boldsymbol{E}^{p}_{t}$ is the prescribed emissions, which can be obtained from the emissions inventories. Therefore, the forecast variables contain the mass concentration $\mathbf{C}$ and the emissions scaling factor λ. The mass concentration $\mathbf{C}$ includes the 15 WRF-Chem/GOCART (Goddard Chemistry Aerosol Radiation and Transport) aerosol variables, and emissions scaling factors include $\lambda^{f}_{PM2.5}$, λ^{f}_{SO2}, λ^{f}_{NO}, and λ^{f}_{NH3}.

During the assimilation stage, both the mass concentration $\mathbf{C}$ and the emissions scaling factor λ are jointly assimilated using the ensemble square root filter (EnSRF) approach, as in Peng et al. (2017). After data assimilation, the state vector $\mathbf{x}$ ($\mathbf{x} = [\mathbf{C}, \lambda]^{T}$) is updated. Then, the analysis of emissions $\left(\boldsymbol{E}^{a}_{i,t}\right)$ is obtained from the prescribed emissions ($\boldsymbol{E}^{p}_{t}$) multiplied by the analysis of scaling factors ($\lambda^{a}_{i,t}$):

$$\boldsymbol{E}^{a}_{i,t} = \lambda^{a}_{i,t}\boldsymbol{E}^{p}_{t}. \tag{6}$$

For a more detailed description of the emissions data assimilation, refer to Peng et al. (2017).

2.2. Data

Surface synoptic observations (SYNOP) from the Automated Data Processing Global Upper Air and Surface Weather Observations provided by the National Centers for Environmental Prediction were employed to evaluate the uncertainties in the simulation of meteorological conditions. The hourly $PM_{2.5}$ concentrations were obtained from the Ministry of Environmental Protection of China (http://113.108.142.147:20035/emcpublish/). These data have been used in several studies on aerosol data assimilation, such as Peng et al. (2017), Zhang et al. (2016), Jiang et al. (2013), and Li et al. (2013). Altogether, 76 stations were selected for the assimilation experiments (black dots in Figure 1), and the other 131 stations were used as independent validation stations (red dots in Figure 1).

Observation errors contain measurement errors and representativeness errors, and these can be calculated following Elbern et al. (2007), Pagowski et al. (2010), Schwartz et al. (2012), and Peng et al. (2017). The

measurement error ε_0 was computed using $\varepsilon_0 = 1.5 + 0.0075 \times \Pi_0$, where Π_0 denotes observational values for $PM_{2.5}$ ($\mu g/m^3$). The representativeness error ε_r depends on the resolution of the model and the locations of the observation sites and was calculated using $\varepsilon_r = r\varepsilon_0\sqrt{\Delta x/L}$, where r is an adjustable parameter (here $r = 0.5$), Δx is the grid spacing (here 12 km), and L is the radius of influence of an observation (here L was set to 3 km). The total $PM_{2.5}$ error (ε_t) was defined as $\varepsilon_t = \sqrt{\varepsilon_0{}^2 + \varepsilon_r{}^2}$. The observation errors were assumed to be uncorrelated so that **R** is a diagonal matrix.

2.3. Experimental Design

The model domain was 1,200 × 1,200 km^2 on a Lambert conformal map projection centered at (39.9°N, 116.4°E), with a 12-km horizontal spacing and 57 vertical levels. The Regional Atmospheric Chemistry Mechanism Scheme (Stockwell et al., 1997) and the Goddard Chemistry Aerosol Radiation and Transport (Chin et al., 2000, 2002) were employed to simulate the gaseous chemistry and aerosol, respectively. The physical parameterizations used in this study included the Rapid Radiative Transfer Model for longwave radiation simulation and the Goddard shortwave radiation scheme, the Yonsei University planetary boundary layer scheme (Hong et al., 2006), and the Grell-3D cumulus parametrization. The prior anthropogenic emissions used in this study came from the Intercontinental Chemical Transport Experiment-Phase B (INTEX-B), which has a 0.5° * 0.5° horizontal resolution and used an improved, detailed technology-based approach to estimate emissions in China (Li, McLinden, et al., 2017; Zhang et al., 2009). Biogenic (Guenther et al., 1995), dust (Ginoux et al., 2001), dimethyl sulfide, and sea salt emissions (Chin et al., 2000, 2002) were calculated online. The meteorological initial conditions and boundary conditions were constructed from the analysis of the National Centers for Environmental Prediction Global Forecast System.

The configuration of the EnSRF settings followed previous studies (Peng et al., 2017; Schwartz et al., 2012; Whitaker & Hamill, 2002). There were 50 ensemble members. The horizontal covariance localization radius was set as 607.5 km, and the posterior (after assimilation) multiplicative inflation factor was set as 1.2 for all the concentration analysis. Four-day forecasting of the 50-member ensembles was performed from 0000 UTC on 1 August to 2300 UTC on 4 August 2015 to initialize and spin up the ensemble forecasts. The ensemble members were generated by adding Gaussian random noise with a zero mean and static background error covariances (Torn et al., 2006). The chemical initial conditions were set to 0, representing clean conditions, as described by Liu et al. (2011). The chemical boundary conditions were idealized profiles embedded within the WRF-Chem model. The emissions for each member were created by adding zero mean random noises to the anthropogenic emissions, as reported by Schwartz et al. (2014). Also, the variances were set to 10% of the prior anthropogenic emissions. These perturbed emissions were used only during the spin-up period of the ensemble forecast.

The assimilation experiment was conducted from 0000 UTC on 5 August 2015 to 0000 UTC on 10 September 2015. The assimilation cycle interval was 1 hr. The first 50 ensemble chemical fields were drawn from the spin-up ensemble forecast valid at 0000 UTC on 5 August 2015. In the subsequent assimilation cycles, the initial conditions for the chemical variables of each member were drawn from the updated chemical fields of the previous cycle. The aerosol lateral boundary conditions of each member were idealized profiles embedded within the WRF-Chem model. As for the meteorological ensemble fields, the lateral boundary conditions were prepared in advance. The initial conditions of each member of the meteorological fields were drawn from the forecast meteorological fields of the previous cycle before re-centering with the Global Forecast System analysis because we did not carry out meteorological analysis.

Using the prior anthropogenic emissions as the source input, a control experiment (CTRL) was conducted to simulate the variation of $PM_{2.5}$ concentrations from 0000 UTC on 5 August 2015 to 0000 UTC on 10 September 2015. To further evaluate the impact of emissions assimilation and the emissions regulations of different intensity and strategy on the simulated $PM_{2.5}$ concentrations, another three sensitivity simulations were also performed during the same period. All the settings for these sensitivity experiments were the same, except for their emissions inputs. The emissions inputs for the three sensitivity experiments were derived from the assimilated emissions during the preregulations period (6–19 August 2015, SENS01), during the regular-regulations period (20–27 August 2015, SENS02), and during the stringent-regulations period (1–3 September 2015, SENS03), respectively.

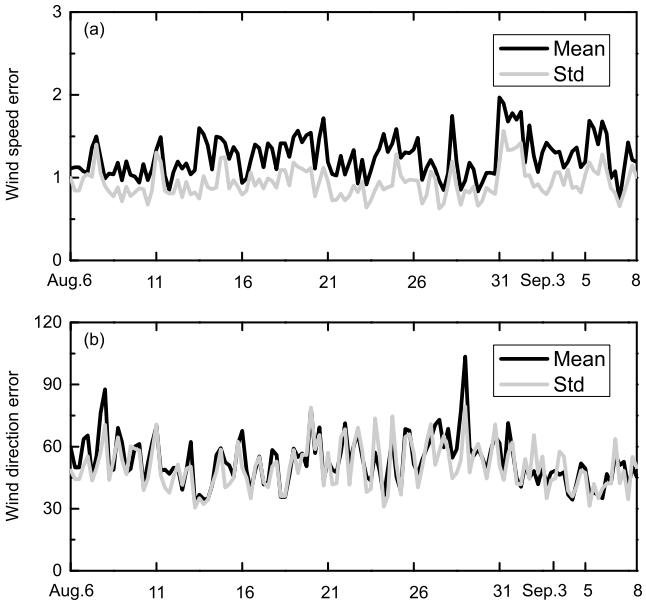

Figure 2. Evolution of the mean and standard deviations of surface wind errors every 6 hr verified against the 74 surface synoptic observations sites within the model domain from 0000 UTC (Beijing standard time) on 6 August to 0000 UTC on 8 September: (a) wind speed errors, units: m/s; (b) wind direction errors, units: degree.

3. Numerical Results

3.1. Validation of the Emissions Data Assimilation System

The modeled meteorological conditions play an important role in the constraint of emissions; larger wind errors are usually assumed to affect the simulation of pollutant transport and thus influence the accuracy of the derived emissions. Beijing locates to the southwest of Yanshan Mountain, to the east of Taihang Mountain. And there are large heavy industrial regions to the south of Beijing. As a result, high $PM_{2.5}$ concentrations in Beijing always correspond to the southerly wind, while low $PM_{2.5}$ concentrations in Beijing usually correspond to the northerly wind because of the specific terrain and the distribution of polluted industries (Gao et al., 2011). Therefore, the accurate simulation of wind direction is also very important in the emission data assimilation within this region. To quantitatively evaluate the accuracy of the simulated meteorological conditions, the simulated grid surface winds are interpolated on the 74 SYNOP (surface synoptic observations) sites within the model domain and are compared with the surface wind observations. Figure 2 shows the mean of the absolute errors of the surface wind speed and direction every 6 hr, as well as their standard deviations. The mean absolute errors during the whole simulation period are 1.25 m/s and 52.78° for surface wind speed and direction, respectively. The magnitudes of surface wind speed error are quite similar to the analysis error of the high-resolution regional mesoscale forecast system (Wei et al., 2010). The magnitudes of surface wind direction error are between 1/2 and 2/3 quarter, which are insufficient to change the direction of the prevailing wind. It should be noted that there are considerable absolute wind direction errors (close to 90°) at several individual times, which might cause uncertainties in the emission assimilation. However, the wind forecast errors were generally within an acceptable range during the whole simulation period.

It is important and necessary to assess the ensemble spread for an ensemble-based data assimilation system. The time series of the ensemble spread of the scaling factors for $PM_{2.5}$ were calculated by averaging the values of each grid within the domain at 1-hr intervals (Figure 3). The ensemble spread of the scaling factor for $PM_{2.5}$ was stably distributed around 0.5 during the 1-month simulation, which indicates that the uncertainties of the ensemble emissions were about 50%. Since the emissions of SO_2, NO, and NH_3 were derived from $PM_{2.5}$ observations in the current data assimilation system, there were relatively larger uncertainties in their inversions (figures not shown). In future work, the specific observations of SO_2, NO, and NH_3 will be used to improve the estimation of their emissions. The grid-scale ensemble spreads in Beijing and the south Beijing-Tianjin-Hebei (BTH) are around 0.5 (Figure S1 in the supporting information). Although there are slightly larger ensemble spreads in the southern boundary, they decayed with the integration and were assumed to have little impact on the emission estimation in Beijing and the BTH region.

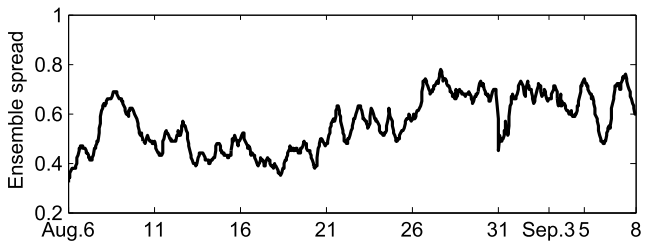

Figure 3. Time series of the domain-averaged ensemble spread for the scaling factors of $PM_{2.5}$, SO_2, NO, and NH_3 from 0000 BST on 6 August to 0000 BST on 8 September.

As introduced earlier, the CTRL experiment used the prior anthropogenic emissions as the source input, while the emissions inputs of the SESN01 experiment were derived from the assimilated emissions during the preregulations period (6–19 August 2015). Therefore, comparison between the CTRL and SENS01 experiments could illustrate the improvement in the simulation of $PM_{2.5}$ concentrations through emissions data assimilation. Figure 4 shows the observed $PM_{2.5}$ concentrations alongside the simulated $PM_{2.5}$ concentrations in the CTRL and SENS01 experiments, in the south BTH region and in Beijing, separately. After emissions data assimilation, the simulated $PM_{2.5}$ concentrations in the SENS01 experiment were closer to the observational values than those in the CTRL experiment. Moreover, both experiments were able to represent the variation of $PM_{2.5}$ concentrations, and the overall

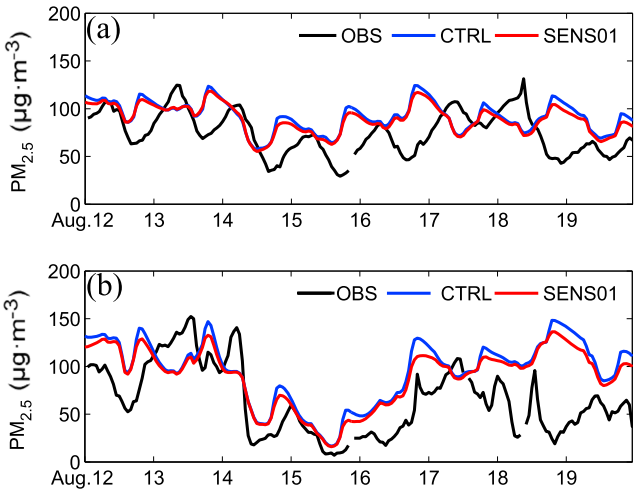

Figure 4. Time series of the hourly $PM_{2.5}$ concentrations during the simulation period prior to the regulations being implemented (0000 BST on 12 August to 0000 BST on 20 August), in (a) the south Beijing-Tianjin-Hebei region and (b) Beijing, obtained from observations (OBS) and the control (CTRL) and SENS01 experiments.

errors were small and acceptable. Interestingly, the largest mismatch appeared on 19 August, which may be attributable to the large simulated wind errors on that day (Figure 2).

To sum up, the derived emissions during the whole simulation were reasonable, except that there may have been notable uncertainties at individual times due to the large meteorological errors.

3.2. Emissions Estimation

Figure 5a shows the daily average prior anthropogenic emissions based on equally allocating the 2006 emissions inventory in August 2016 (Zhang et al., 2009), and Figure 5b presents the updated mean emissions after assimilation and before the regulations (0000 BST on 6 August to 2300 BST on 12 August). Similarly, Figures 5c and 5d show the assimilated mean emissions during the regular-regulations period (0000 BST on 20 August to 2300 BST on 30 August) and stringent-regulations period (0000 BST on 1 August to 2300 BST on 2 September), respectively. Furthermore, the differences between the updated emissions during these stages and the prior anthropogenic emissions are depicted in Figures 5e–5g, respectively. There were several major emissions sources in south Beijing, Tianjin, south and east Hebei province, central Shanxi province, and Shandong province, which are all major industrial or high-density urban areas (Figures 5a and 5b). Before the regulations, the emissions in north China were generally reduced after assimilation, especially in several major source areas (Figure 5e). The emissions decreased remarkably with an increase in the intensity of the regulations. During the regular-regulations period, the emissions reduction was mainly located in Beijing, Tianjin, and several large cities of Hebei, Shanxi, and Shandong provinces. However, the most remarkable emissions reductions occurred during the stringent-regulations period, with the emissions reduction extending to the whole southern part of Hebei province and the west of Shandong province. Furthermore, the amplitude of emissions reduction within all the regulated regions was largest during the stringent-regulations period (Figure 5g).

Figures 6a and 6b present the evolution of the assimilated zonally averaged daily emissions and their differences from the prior anthropogenic emissions, respectively, in the south BTH region (box in Figure 1) from 6 August to 8 September. The averaged emissions and differences between mean emissions and prior emissions showed remarkable differences during the preregulations, regular-regulations, stringent-regulations, and postregulations periods (Figures 6a and 6b). During the preregulations period, there were high emission levels over the whole region. As the regular regulations came into force, emissions over Beijing and its immediate surrounding area consistently reduced. Over time, the area of emissions reduction extended over 38°N to the whole BTH region. The largest amplitude of emissions reduction occurred throughout the whole stringent-regulations period. The emissions reduction even lasted after regulations were lifted; however, the coverage and amplitude of emissions reduction reduced. Figures 6a and 6b show clearly the expansion of the emissions reduction area, as well as the enhancement of the emissions reduction magnitude, as the regulations were enhanced step by step.

The relationship between changes in emissions and the $PM_{2.5}$ concentration is complicated because of the nonlinear chemical and physical processes involved in the formation of secondary $PM_{2.5}$, as well as other factors, such as the meteorological conditions. However, low emissions are vital for good air quality. The time series of the observed mean $PM_{2.5}$ concentration in Beijing and the surrounding region are shown in Figures 6c and 6d, respectively. Generally, the variation in the observed $PM_{2.5}$ concentration coincided with the variation in emissions reduction. Figures 6c and 6d clearly present a higher $PM_{2.5}$ concentration before the regulations were implemented, a much lower $PM_{2.5}$ concentration during the whole regulations period, and even a $PM_{2.5}$ concentration increase immediately after the regulations were halted. Furthermore, the lowest $PM_{2.5}$ concentrations within both the local and surrounding regions were reported when the stringent regulations were in force; the average $PM_{2.5}$ concentrations in Beijing even fell below 10 $\mu g/m^3$.

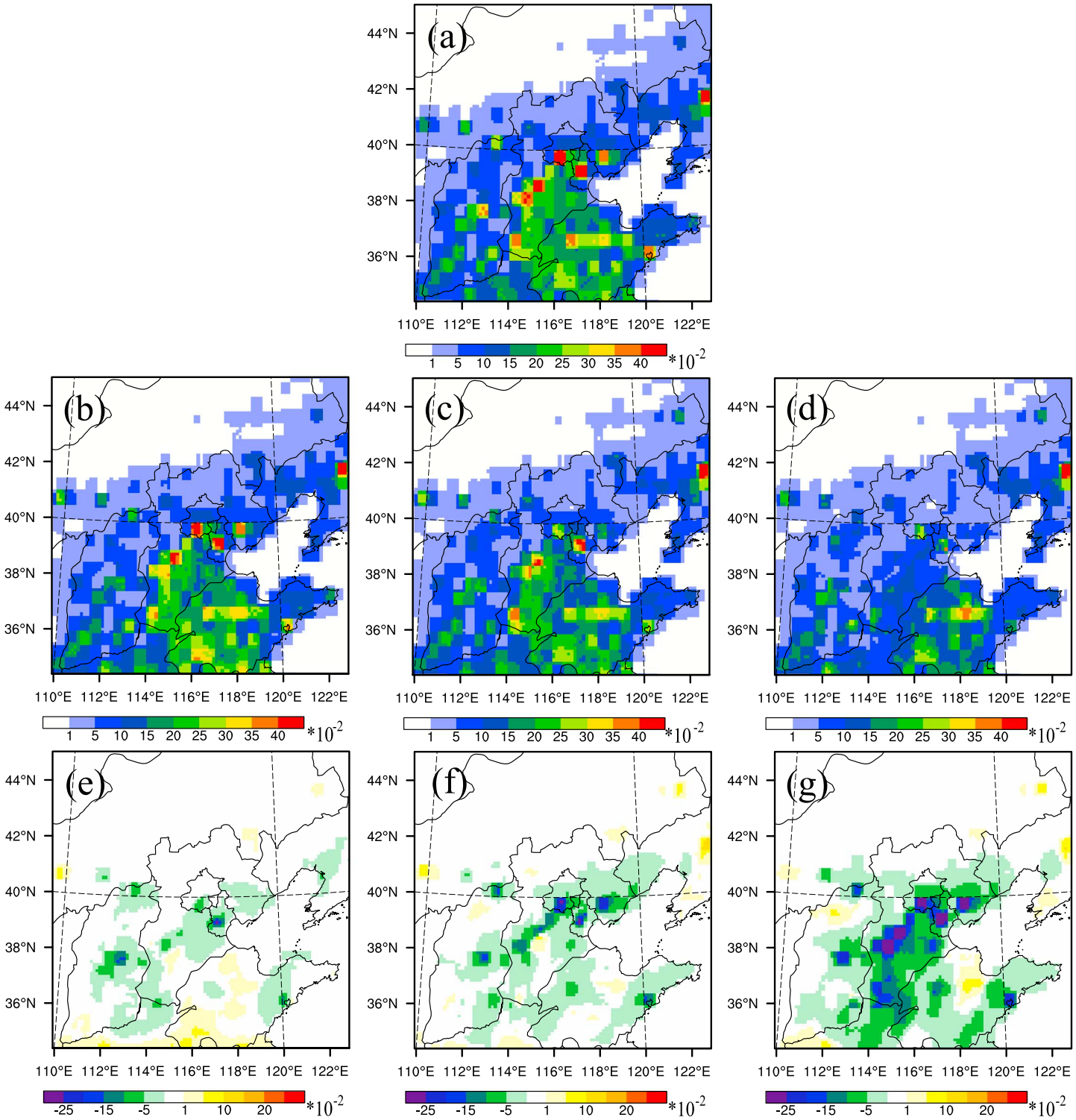

Figure 5. Spatial distribution of (a) the prior unspeciated primary sources of $PM_{2.5}$ ($\mu g \cdot m^{-2} \cdot s^{-1}$) and (b–d) the time-averaged ensemble mean analysis of $PM_{2.5}$ emissions at the lowest model level averaged over all hours during (b) 6–19 August 2015, (c) 20–31 August 2015, and (d) 1–3 September 2015. (e–g) Time-averaged differences between the ensemble mean analysis and the prior values at the lowest model level averaged over all hours during (e) 6–19 August 2015, (f) 20–31 August 2015, and (g) 1–3 September 2015.

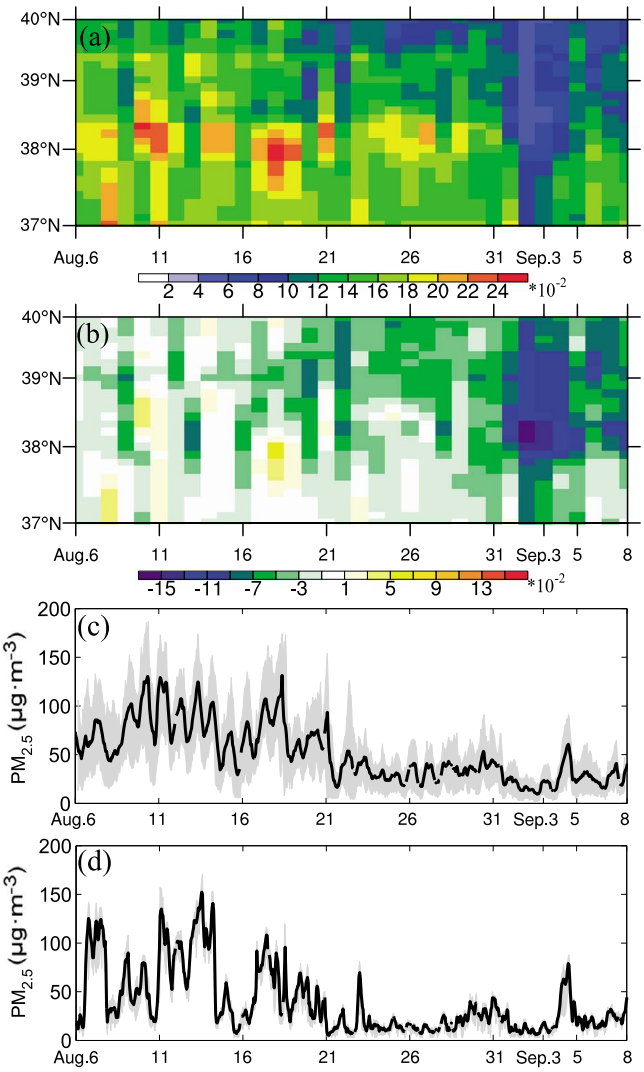

Figure 6. Evolution of the longitudinally averaged (a) ensemble mean analysis of $PM_{2.5}$ emissions ($\mu g \cdot m^{-2} \cdot s^{-1}$) and (b) differences between the ensemble mean analysis and the prior values ($\mu g \cdot m^{-2} \cdot s^{-1}$) over the south Beijing-Tianjin-Hebei (BTH) region marked in Figure 1. (c, d) Time series of the observed mean $PM_{2.5}$ concentration ($\mu g/m^3$) in (c) the south BTH region and (d) Beijing from 0000 BST on 6 August to 0000 BST on 8 September. Shaded backgrounds indicate the distribution of observations, where the top edge represents the 90th percentile and the bottom edge the 10th percentile.

Figures 7a and 7b present the time series of the hourly and daily mean prior to anthropogenic emissions and the updated emissions in the south BTH region marked in Figure 1, respectively. With the enhancement of the regulations, the emissions decreased both in daytime and at nighttime, with the largest decline occurring in daytime since most emissions occur during the day. The daily mean value of the prior unspeciated primary sources of $PM_{2.5}$ was 21.35 $\mu g \cdot m^{-2} \cdot s^{-1}$. The mean values of the assimilated emissions were 19.67, 16.98, 10.81, and 13.98 $\mu g \cdot m^{-2} \cdot s^{-1}$ (about 92%, 79.6%, 50.7%, and 65.5% of the prior anthropogenic emissions) for the days during the preregulations, regular-regulations, stringent-regulations, and postregulations periods, respectively. The corresponding standard deviations were 1.66, 1.37, 3.12, and 1.17 $\mu g \cdot m^{-2} \cdot s^{-1}$, respectively.

3.3. Sensitivity Experiments

The above analysis shows that emissions data assimilation based on the EnSRF approach provides a reasonable estimation of the actual emissions during different stages of a period with emissions regulations. In this next section, the impact of different emissions inputs on the simulation of $PM_{2.5}$ concentrations is discussed. The impact of the emissions regulations during the different stages was further evaluated with a series of sensitivity simulations that were forced by the updated mean emissions before the regulations and during the regular- and stringent-regulations periods, respectively. The sensitivity experiments were designed to make idealized predictions under the conditions of no emissions regulations, regular regulations, or stringent regulations, throughout the whole simulation.

Figures 8a and 8b show the evolution of the area-averaged $PM_{2.5}$ concentrations in the CTRL and three sensitivity experiments in the south BTH region and Beijing, respectively. The variations of $PM_{2.5}$ concentrations in the four experiments generally coincided with each other and featured remarkable diurnal cycles. However, the magnitudes of the simulated $PM_{2.5}$ concentrations showed large differences in the four experiments. During the whole simulation, the CTRL experiment, in which no regulations were implemented, showed the highest $PM_{2.5}$ concentrations, whereas experiment SENS02—with the most intense regulations—showed the lowest $PM_{2.5}$ concentrations. It should be noted that the $PM_{2.5}$ concentrations decreased substantially on 1 September regardless of whether the emissions regulations were implemented, indicating that meteorological conditions might have played an important role in pollutant transport during this period. As an evidence, Kang et al. (2016) showed that the prevailing wind direction in BTH was northern wind due to the existence of a northeast cold vortex from 1 September on, which was beneficial for the low $PM_{2.5}$ concentrations.

The responses of the simulated $PM_{2.5}$ concentrations to different emissions inputs can be further illustrated by the averaged diurnal variations of the simulated $PM_{2.5}$ concentrations during the whole simulation period in the south BTH region and in Beijing (Figure 9). In the scenario of stringent regulations, the $PM_{2.5}$ concentrations, both in the daytime and at nighttime, were much smaller than those in the other scenarios. It should also be noted that the differences among the four experiments were largest in the middle of the night and smallest in the afternoon. Since the height of the nocturnal stable boundary layer is generally about 10% of that of the daytime convective boundary layer, emissions are less dispersive at nighttime. Therefore, the simulated $PM_{2.5}$ concentrations in the daytime showed smaller difference than those at nighttime.

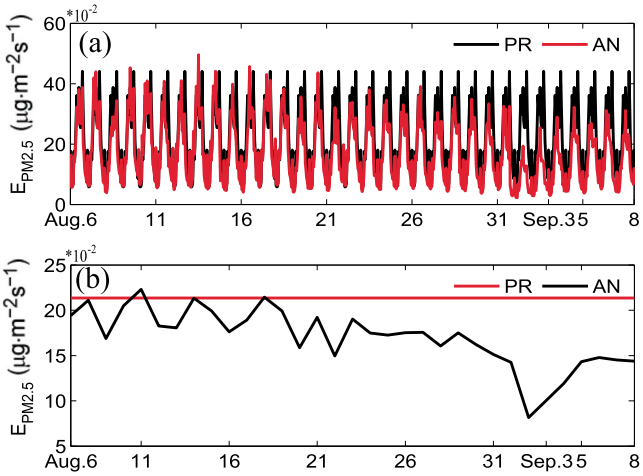

Figure 7. (a) Hourly and (b) daily area-averaged time series of the prior unspeciated primary sources of $PM_{2.5}$ ($\mu g \cdot m^{-2} \cdot s^{-1}$; black) and the analyzed unspeciated primary $PM_{2.5}$ emissions (red) in the south Beijing-Tianjin-Hebei region from 0000 BST on 6 August to 0000 BST on 8 September.

The spatial distribution of the simulated $PM_{2.5}$ concentrations in all four experiments is illustrated in Figure 10. In the scenario that no control measures were implemented, a high $PM_{2.5}$ concentration belt emerged from Beijing and Tianjin and spread to southern Hebei province and western Shandong province (Figures 10a and 10b). Compared with the CTRL experiment, the magnitudes of the $PM_{2.5}$ concentrations were moderately reduced after emissions assimilation (SENS01), especially within the high-pollution belt. The difference between the CTRL and SENS01 experiments was consistent with the modifications of the prior emissions through emissions assimilation (Figures 5a, 5b, and 5e). The $PM_{2.5}$ concentrations in the simulated high-$PM_{2.5}$ concentration belt reduced substantially in the simulation under the scenario of regular regulations (Figure 10c), and if the stringent regulations were implemented during the whole period the $PM_{2.5}$ concentration reduced even more, with the belt also narrowing considerably—especially in Beijing and Tianjin (Figure 10a). The sensitivity experiments under the different scenarios further highlighted the valuable role played by emissions regulations at different intensities in reducing $PM_{2.5}$ concentrations. More intense emissions regulation will lead to better air quality.

4. Summary and Discussion

In order to guarantee good air quality for the 15th International Association of Athletics Federations World Championships (22–30 August) and the China Victory Day parade (3 September) in Beijing, comprehensive emissions regulations at different intensity levels were implemented by the government for about half a month. As a result, the air quality of Beijing remained good for 15 consecutive days during this period, and the $PM_{2.5}$ concentrations of the adjacent provinces were also largely reduced. Emissions data assimilation based on EnSRF was conducted to estimate the actual emissions during this period. Sensitivity simulations forced with the updated emissions before the regulations, during the regular- and stringent-regulations periods, and after the regulations were halted were used to further evaluate the impact of the regulations under different strategy and intensity scenarios on the air quality. The main conclusions are as follows:

1. The emissions data assimilation system based on EnSRF was able to estimate reasonably the variations of the anthropogenic emissions before, during, and after implementation of the emissions regulations. The emissions regulations greatly reduced the anthropogenic emissions; not only did the emissions reduction area expand, but the emissions reduction magnitude also decreased considerably with the step-by-step enhancement of the regulations. The updated emissions were about 80% and 50% of the prior anthropogenic emissions during the regular- and stringent-regulations periods, respectively. The benefits of the regulations lasted for several days after the end of the regulations period.
2. The variations of $PM_{2.5}$ concentrations in Beijing and the surrounding region were consistent with those of the emissions. The $PM_{2.5}$ concentrations consistently decreased during the regulations period, and the lowest $PM_{2.5}$ concentrations occurred during the stringent-regulations period.
3. Sensitivity experiments further highlighted the valuable impacts of different strategies for emissions regulations.

In addition to emission controls, meteorological conditions sometimes can also play a significant role in producing low aerosol concentrations during the Beijing Olympic Games (Gao et al., 2011; Xing et al., 2011). In

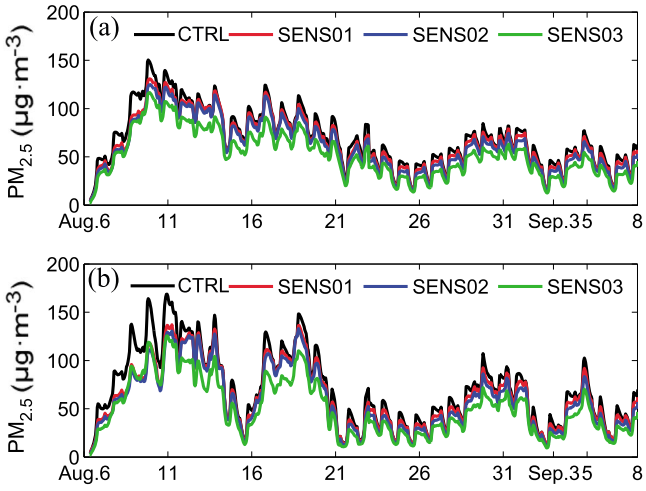

Figure 8. Time series of the hourly pollutant concentrations averaged (a) over the south Beijing-Tianjin-Hebei region and (b) over Beijing obtained from the control (CTRL) and three sensitivity experiments from 0000 BST on 6 August to 0000 BST on 8 September.

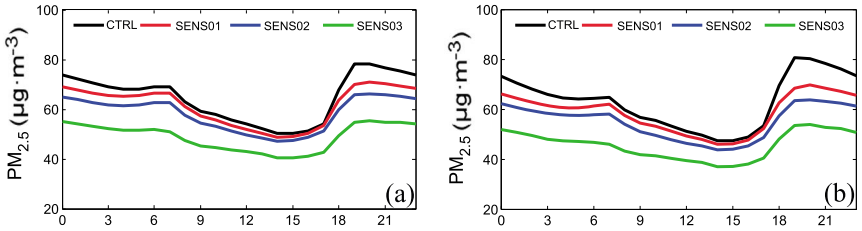

Figure 9. Averaged diurnal variations of the simulated $PM_{2.5}$ concentrations in the four experiments during the whole simulation period in (a) the south Beijing-Tianjin-Hebei region and (b) Beijing. Times are in Beijing standard time.

this study, the $PM_{2.5}$ concentrations decreased substantially from 1 September regardless of what kind of emissions regulations were implemented or not, which was ascribed to the proper meteorological conditions (Kang et al., 2016; Xue et al., 2017). However, a persistent reduction in $PM_{2.5}$ surface concentrations will depend on a consistent reduction in anthropogenic emissions.

Except for the meteorological conditions, the prior emission inventory is another important issue related to the accuracy of the emission estimation. Fan et al. (2018) noted that the aerosol loadings in China are often underestimated in global climate models; one reason is the uncertainties in the emission inventory, which is closely related to the atmospheric loadings of primary aerosols. Furthermore, fast-paced economy and environmental

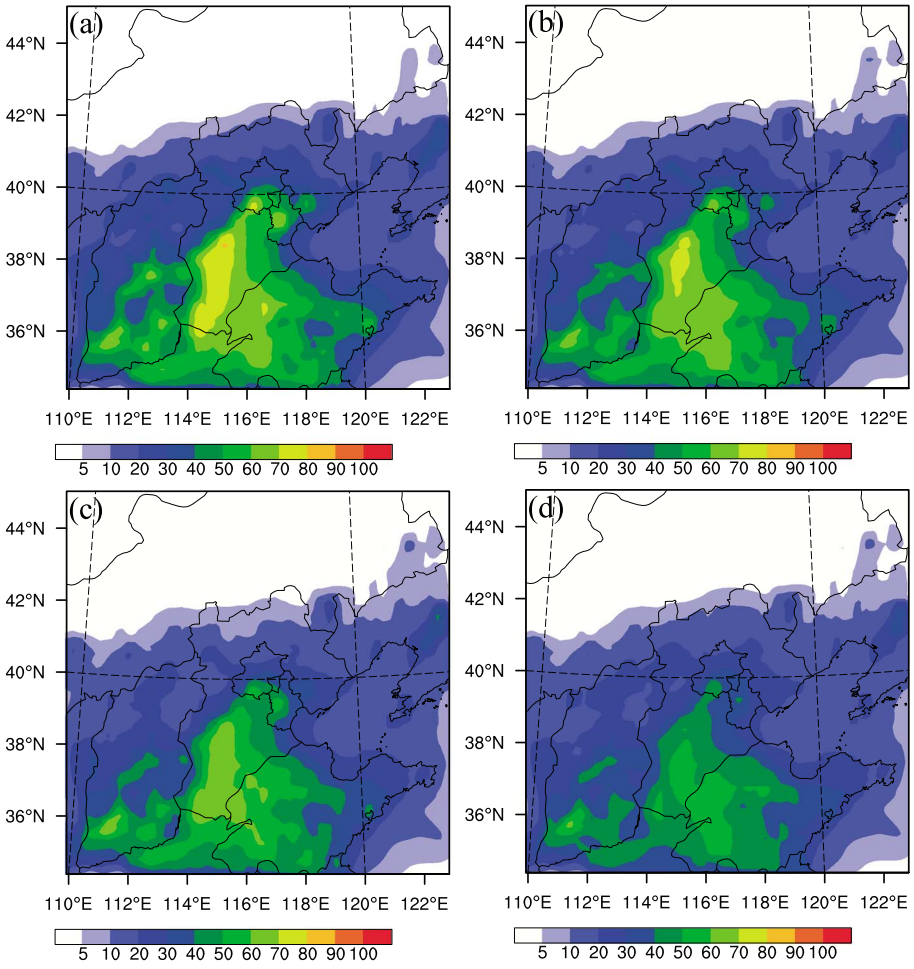

Figure 10. Spatial distribution of the $PM_{2.5}$ mass ($\mu g/m^3$) of the (a) control, (b) SEN01, (c) SEN02, and (d) SEN03 experiments at the lowest model level averaged over all hours from 0000 BST on 20 August to 0000 BST on 3 September.

policy will also lead to unforeseen emission changes (Li, Liu, et al., 2017). There are many bottom-up anthropogenic emission inventories (Li, McLinden, et al., 2017), such as Intercontinental Chemical Transport Experiment-Phase B (Zhang et al., 2009), Transport and Chemical Evolution over the Pacific (Streets et al., 2003), Regional Emission Inventory in Asia Version 1.1 (Ohara et al., 2007), Multi-resolution Emission Inventory for China (Lei et al., 2011; Li et al., 2014), and so on. Large differences exist among the current bottom-up anthropogenic emission inventories, due to the treatment in changes of activity rates and emission factors with China's rapid economic development and application of air pollution control technologies (Yang et al., 2013; Li, Liu, et al., 2017). In this study, the INTEX-B inventory was used as the prior emission with our previous work consistent. However, it is scientifically interesting to evaluate the value and effect of different emission inventories in the emission assimilation procedures. Besides the above factors, the uncertainties in the emission assimilation may also arise in other aspects, such as model parameterized physics, spatial and vertical resolution, and vertical mixing and chemical processes, which need further investigation.

Acknowledgments
The authors are grateful to the two anonymous reviewers for their precious suggestions. This work was supported by the National Key Technologies Research and Development Program of China (2016YFC0202102), the National Natural Science Foundation of China (41575141), and Natural Science Foundation of Jiangsu Province China (BK20161395). NCAR is sponsored by the U.S. National Science Foundation. This work was also supported by the Nanjing University "Deng Feng" Distinguished Scholars Program (Level B) and the Jiangsu Distinguished Professorship Program. The hourly $PM_{2.5}$ concentrations were obtained from the Ministry of Environmental Protection of China (http://113.108.142.147:20035/emcpublish/) and are provided as supporting information. The numerical calculations in this paper were carried out on the IBM Blade cluster system in the High Performance Computing Center (HPCC) of Nanjing University.

References

Barbu, A. L., Segers, A. J., Schaap, M., Heemink, A. W., & Builtjes, P. J. H. (2009). A multi-component data assimilation experiment directed to sulphur dioxide and sulphate over Europe. *Atmospheric Environment*, *43*(9), 1622–1631. https://doi.org/10.1016/j.atmosenv.2008.12.005

Chai, T., Carmichael, G. R., Tang, Y., Sandu, A., Hardesty, M., Pilewskie, P., et al. (2007). Four dimensional data assimilation experiments with International Consortium for Atmospheric Research on Transport and Transformation ozone measurements. *Journal of Geophysical Research*, *112*, D12S15. https://doi.org/10.1029/2006JD007763

Chan, C. K., & Yao, X. (2008). Air pollution in mega cities in China. *Atmospheric Environment*, *42*(1), 1–42. https://doi.org/10.1016/j.atmosenv.2007.09.003

Chen, R. S., De Sherbinin, A., Ye, C., & Shi, G. Q. (2014). China's soil pollution: Farms on the frontline. *Science*, *344*(6185), 691–691. https://doi.org/10.1126/science.344.6185.691-a

Chin, M., Ginoux, P., Kinne, S., Torres, O., Holben, B. N., Duncan, B. N., et al. (2002). Tropospheric aerosol optical thickness from the GOCART model and comparisons with satellite and Sun photometer measurements. *Journal of the Atmospheric Sciences*, *59*(3), 461–483. https://doi.org/10.1175/1520-0469(2002)059%3C0461:TAOTFT%3E2.0.CO;2

Chin, M., Rood, R. B., Lin, S. J., Muller, J. F., & Thompson, A. M. (2000). Atmospheric sulfur cycle simulated in the global model GOCART: Model description and global properties. *Journal of Geophysical Research*, *105*(D20), 24,671–24,687. https://doi.org/10.1029/2000JD900384

Constantinescu, E. M., Sandu, A., Chai, T., & Carmichael, G. R. (2007a). Ensemble-based chemical data assimilation. I: General approach. *Quarterly Journal of the Royal Meteorological Society*, *133*, 1229–1243.

Constantinescu, E. M., Sandu, A., Chai, T., & Carmichael, G. R. (2007b). Ensemble-based chemical data assimilation. II: Covariance localization. *Quarterly Journal of the Royal Meteorological Society*, *133*, 1245–1256.

Ding, J., van der A, R. J., Mijling, B., Levelt, P. F., & Hao, N. (2015). NO_x emission estimates during the 2014 Youth Olympic Games in Nanjing. *Atmospheric Chemistry and Physics*, *15*(16), 9399–9412. https://doi.org/10.5194/acp-15-9399-2015

Elbern, H., Strunk, A., Schmidt, H., & Talagrand, O. (2007). Emission rate and chemical state estimation by 4-dimensional variational inversion. *Atmospheric Chemistry and Physics*, *7*(14), 3749–3769. https://doi.org/10.5194/acp-7-3749-2007

Fan, T., Liu, X., Ma, P.-L., Zhang, Q., Li, Z., Jiang, Y., et al. (2018). Emission or atmospheric processes? An attempt to attribute the source of large bias of aerosols in eastern China simulated by global climate models. *Atmospheric Chemistry and Physics*, *18*, 1395–1417. https://doi.org/10.5194/acp-18-1395-2018

Gao, Y., Liu, X., Zhao, C., & Zhang, M. (2011). Emission controls versus meteorological conditions in determining aerosol concentrations in Beijing during the 2008 Olympic Games. *Atmospheric Chemistry and Physics*, *11*(23), 12,437–12,451. https://doi.org/10.5194/acp-11-12437-2011

Ginoux, P., Chin, M., Tegen, I., Prospero, J. M., Holben, B., Dubovik, O., & Lin, S. J. (2001). Sources and distributions of dust aerosols simulated with the GOCART model. *Journal of Geophysical Research*, *106*(D17), 20,255–20,273. https://doi.org/10.1029/2000JD000053

Grell, G., Peckham, S. E., Schmitz, R., McKeen, S. A., Frost, G., Skamarock, W. C., & Eder, B. (2005). Fully coupled "online" chemistry within the WRF model. *Atmospheric Environment*, *39*(37), 6957–6975. https://doi.org/10.1016/j.atmosenv.2005.04.027

Guenther, A., Hewitt, C. N., Erickson, D., Fall, R., Geron, C., Graedel, T., et al. (1995). A global-model of natural volatile organic-compound emissions. *Journal of Geophysical Research*, *100*(D5), 8873–8892. https://doi.org/10.1029/94jd02950

Guerrette, J. J., & Henze, D. K. (2015). Development and application of the WRFPLUS-Chem online chemistry adjoint and WRFDA-Chem assimilation system. *Geoscientific Model Development*, *8*(6), 1857–1876. https://doi.org/10.5194/gmd-8-1857-2015

Hakami, A., Henze, D. K., Seinfeld, J. H., Chai, T., Tang, Y., Carmichael, G. R., & Sandu, A. (2005). Adjoint inverse modeling of black carbon during the Asian Pacific Regional Aerosol Characterization Experiment. *Journal of Geophysical Research*, *110*, D14301. https://doi.org/10.1029/2004JD005671

Han, X. K., Guo, Q. J., Liu, C. Q., Strauss, H., Yang, J. X., Hu, J., et al. (2016). Effect of the pollution control measures on $PM_{2.5}$ during the 2015 China Victory Day parade: Implication from water-soluble ions and sulfur isotope. *Environmental Pollution*, *218*, 230–241. https://doi.org/10.1016/j.envpol.2016.06.038

Heemink, A. W., & Segers, A. J. (2002). Modeling and prediction of environmental data in space and time using Kalman filtering. *Stochastic Environmental Research and Risk Assessment*, *16*(3), 225–240. https://doi.org/10.1007/s00477-002-0097-1

Henze, D. K., Hakami, A., & Seinfeld, J. H. (2007). Development of the adjoint of GEOS-Chem. *Atmospheric Chemistry and Physics*, *7*(9), 2413–2433. https://doi.org/10.5194/acp-7-2413-2007

Henze, D. K., Seinfeld, J. H., & Shindell, D. T. (2009). Inverse modeling and mapping US air quality influences of inorganic $PM_{2.5}$ precursor emissions using the adjoint of GEOS-Chem. *Atmospheric Chemistry and Physics*, *9*(16), 5877–5903. https://doi.org/10.5194/acp-9-5877-2009

Hong, S. Y., Noh, Y., & Dudhia, J. (2006). A new vertical diffusion package with an explicit treatment of entrainment processes. *Monthly Weather Review*, *134*(9), 2318–2341. https://doi.org/10.1175/Mwr3199.1

Huang, K., Zhang, X. Y., & Lin, Y. F. (2015). The "APEC blue" phenomenon: Regional emission control effects observed from space. *Atmospheic Research*, *164-165*, 65–75. https://doi.org/10.1016/j.atmosres.2015.04.018

Huneeus, N., Boucher, O., & Chevallier, F. (2013). Atmospheric inversion of SO_2 and primary aerosol emissions for the year 2010. *Atmospheric Chemistry and Physics*, *13*(13), 6555–6573. https://doi.org/10.5194/acp-13-6555-2013

Huneeus, N., Chevallier, F., & Boucher, O. (2012). Estimating aerosol emissions by assimilating observed aerosol optical depth in a global aerosol model. *Atmospheric Chemistry and Physics*, *12*(10), 4585–4606. https://doi.org/10.5194/acp-12-4585-2012

Jiang, Z., Liu, Z., Wang, T., Schwartz, C. S., Lin, H.-C., & Jiang, F. (2013). Probing into the impact of 3DVAR assimilation of surface PM_{10} observations over China using process analysis. *Journal of Geophysical Research: Atmospheres*, *118*, 6738–6749. https://doi.org/10.1002/jgrd.50495

Kang, Z., Gui, H., Jiang, Q., & Lu, M. (2016). Characteristics and cause of the "parade blue" in Beijing 2015. *China Environmental Science*, *36*(11), 3227–3226.

Lei, Y., Zhang, Q., He, K. B., & Streets, D. G. (2011). Primary anthropogenic aerosol emission trends for China, 1990–2005. *Atmospheric Chemistry and Physics*, *11*(3), 931–954. https://doi.org/10.5194/acp-11-931-2011

Li, C., McLinden, C., Fioletov, V., Krotkov, N., Carn, S., Joiner, J., et al. (2017). India is overtaking China as the world's largest emitter of anthropogenic sulfur dioxide. *Scientific Reports*, *7*(1), 14304. https://doi.org/10.1038/s41598-017-14639-8

Li, M., Liu, H., Geng, G., Hong, C., Liu, F., Song, Y., et al. (2017). Anthropogenic emission inventories in China: A review. *National Science Review*, *4*(6), 834–866. https://doi.org/10.1093/nsr/nwx150

Li, M., Zhang, Q., Streets, D. G., He, K. B., Cheng, Y. F., Emmons, L. K., et al. (2014). Mapping Asian anthropogenic emissions of nonmethane volatile organic compounds to multiple chemical mechanisms. *Atmospheric Chemistry and Physics*, *14*(11), 5617–5638. https://doi.org/10.5194/acp-14-5617-2014

Li, Z., Zang, Z., Li, Q. B., Chao, Y., Chen, D., Ye, Z., et al. (2013). A three-dimensional variational data assimilation system for multiple aerosol species with WRF/Chem and an application to $PM_{2.5}$ prediction. *Atmospheric Chemistry and Physics*, *13*(8), 4265–4278. https://doi.org/10.5194/acp-13-4265-2013

Lin, H., Liu, T., Fang, F., Xiao, J., Zeng, W., Li, X., et al. (2017). Mortality benefits of vigorous air quality improvement interventions during the periods of APEC blue and parade blue in Beijing, China. *Environmental Pollution*, *220*(Pt A), 222–227. https://doi.org/10.1016/j.envpol.2016.09.041

Liu, H. R., Liu, C., Xie, Z. Q., Li, Y., Huang, X., Wang, S. S., et al. (2016). A paradox for air pollution controlling in China revealed by "APEC blue" and "parade blue". *Scientific Reports*, *6*(1), 34408. https://doi.org/10.1038/srep34408

Liu, Z. Q., Liu, Q. H., Lin, H. C., Schwartz, C. S., Lee, Y. H., & Wang, T. J. (2011). Three-dimensional variational assimilation of MODIS aerosol optical depth: Implementation and application to a dust storm over East Asia. *Journal of Geophysical Research*, *116*, D23206. https://doi.org/10.1029/2011JD016159

Miyazaki, K., Eskes, H. J., Sudo, K., Takigawa, M., van Weele, M., & Boersma, K. F. (2012). Simultaneous assimilation of satellite NO_2, O_3, CO, and HNO_3 data for the analysis of tropospheric chemical composition and emissions. *Atmospheric Chemistry and Physics*, *12*(20), 9545–9579. https://doi.org/10.5194/acp-12-9545-2012

Miyazaki, K., Eskes, H. J., Sudo, K., & Zhang, C. (2014). Global lighting NO_x production estimated by an assimilation of multiple satellite data sets. *Atmospheric Chemistry and Physics*, *14*, 3277–3305. https://doi.org/10.5194/acp-14-3277-2014

Ohara, T., Akimoto, H., Kurokawa, J., Horii, N., Yamaji, K., Yan, X., & Hayasaka, T. (2007). An Asian emission inventory of anthropogenic emission sources for the period 1980–2020. *Atmospheric Chemistry and Physics*, *7*(16), 4419–4444. https://doi.org/10.5194/acp-7-4419-2007

Okuda, T., Matsuura, S., Yamaguchi, D., Umemura, T., Hanada, E., Orihara, H., et al. (2011). The impact of the pollution control measures for the 2008 Beijing Olympic Games on the chemical composition of aerosols. *Atmospheric Environment*, *45*(16), 2789–2794. https://doi.org/10.1016/j.atmosenv.2011.01.053

Pagowski, M., Grell, G. A., McKeen, S. A., Peckham, S. E., & Devenyi, D. (2010). Three-dimensional variational data assimilation of ozone and fine particulate matter observations: Some results using the Weather Research and Forecasting-Chemistry model and grid-point statistical interpolation. *Quarterly Journal of the Royal Meteorological Society*, *136*(653), 2013–2024. https://doi.org/10.1002/qj.700

Peng, Z., Liu, Z. Q., Chen, D., & Ban, J. M. (2017). Improving $PM_{2.5}$ forecast over China by the joint adjustment of initial conditions and source emissions with an ensemble Kalman filter. *Atmospheric Chemistry and Physics*, *17*(7), 4837–4855. https://doi.org/10.5194/acp-17-4837-2017

Schutgens, N. A. J., Miyoshi, T., Takemura, T., & Nakajima, T. (2010). Sensitivity tests for an ensemble Kalman filter for aerosol assimilation. *Atmospheric Chemistry and Physics*, *10*(14), 6583–6600. https://doi.org/10.5194/acp-10-6583-2010

Schwartz, C. S., Liu, Z. Q., Lin, H. C., & Cetola, J. D. (2014). Assimilating aerosol observations with a "hybrid" variational-ensemble data assimilation system. *Journal of Geophysical Research: Atmospheres*, *119*, 4043–4069. https://doi.org/10.1002/2013JD020937

Schwartz, C. S., Liu, Z. Q., Lin, H. C., & McKeen, S. A. (2012). Simultaneous three-dimensional variational assimilation of surface fine particulate matter and MODIS aerosol optical depth. *Journal of Geophysical Research*, *117*, D13202. https://doi.org/10.1029/2011JD017383

Sekiyama, T. T., Tanaka, T. Y., Shimizu, A., & Miyoshi, T. (2010). Data assimilation of CALIPSO aerosol observations. *Atmospheric Chemistry and Physics*, *10*(1), 39–49. https://doi.org/10.5194/acp-10-39-2010

Stockwell, W. R., Kirchner, F., Kuhn, M., & Seefeld, S. (1997). A new mechanism for regional atmospheric chemistry modeling. *Journal of Geophysical Research*, *102*(D22), 25,847–25,879. https://doi.org/10.1029/97JD00849

Streets, D. G., Bond, T. C., Carmichael, G. R., Fernandes, S. D., Fu, Q., He, D., et al. (2003). An inventory of gaseous and primary aerosol emissions in Asia in the year 2000. *Journal of Geophysical Research*, *108*(D21), 8809. https://doi.org/10.1029/2002JD003093

Streets, D. G., Fu, J. S., Jang, C. J., Hao, J., He, K., Tang, X., et al. (2007). Air quality during the 2008 Beijing Olympic Games. *Atmospheric Environment*, *41*(3), 480–492. https://doi.org/10.1016/j.atmosenv.2006.08.046

Tang, G., Zhu, X., Hu, B., Xin, J., Wang, L., Munkel, C., et al. (2015). Impact of emission controls on air quality in Beijing during APEC 2014: Lidar ceilometer observations. *Atmospheric Chemistry and Physics*, *15*(21), 12,667–12,680. https://doi.org/10.5194/acp-15-12667-2015

Tang, X., Zhu, J., Wang, Z. F., & Gbaguidi, A. (2011). Improvement of ozone forecast over Beijing based on ensemble Kalman filter with simultaneous adjustment of initial conditions and emissions. *Atmospheric Chemistry and Physics*, *11*(24), 12,901–12,916. https://doi.org/10.5194/acp-11-12901-2011

Torn, R. D., Hakim, G. J., & Snyder, C. (2006). Boundary conditions for limited-area ensemble Kalman filters. *Monthly Weather Review*, *134*(9), 2490–2502. https://doi.org/10.1175/Mwr3187.1

Wang, G., Cheng, S. Y., Wei, W., Yang, X. W., Wang, X. Q., Jia, J., et al. (2017). Characteristics and emission-reduction measures evaluation of $PM_{2.5}$ during the two major events: APEC and parade. *Science of the Total Environment*, *595*, 81–92. https://doi.org/10.1016/j.scitotenv.2017.03.231

Wang, J., Xu, X. G., Henze, D. K., Zeng, J., Ji, Q., Tsay, S. C., & Huang, J. P. (2012). Top-down estimate of dust emissions through integration of MODIS and MISR aerosol retrievals with the GEOS-Chem adjoint model. *Geophysical Researh Letter*, *39*, L08802. https://doi.org/10.1029/2012GL051136

Wang, P., Wang, H., Wang, Y. Q., Zhang, X. Y., Gong, S. L., Xue, M., et al. (2016). Inverse modeling of black carbon emissions over China using ensemble data assimilation. *Atmospheric Chemistry and Physics*, *16*(2), 989–1002. https://doi.org/10.5194/acp-16-989-2016

Wang, S. L., Gao, J., Zhang, Y. C., Zhang, J. Q., Cha, F. H., Wang, T., et al. (2014). Impact of emission control on regional air quality: An observational study of air pollutants before, during and after the Beijing Olympic Games. *Journal of Environmental Sciences (China)*, *26*(1), 175–180. https://doi.org/10.1016/S1001-0742(13)60395-2

Wang, T., Nie, W., Gao, J., Xue, L. K., Gao, X. M., Wang, X. F., et al. (2010). Air quality during the 2008 Beijing Olympics: Secondary pollutants and regional impact. *Atmospheric Chemistry and Physics*, *10*(16), 7603–7615. https://doi.org/10.5194/acp-10-7603-2010

Wang, X., Liang, X.-Z., Jiang, W., Tao, Z., Wang, J. X.-L., Liu, H., et al. (2010). WRF-Chem simulation of East Asian air quality: Sensitivity to temporal and vertical emissions distributions. *Atmospheric Environment*, *44*, 660–669.

Wei, D., You, F., Fan, S., Yang, B., & Chen, M. (2010). Assessment and analysis of sounding information obtained from Beijing Rapid Update Cycle Forecast System (in Chinese). *Meteorological Monthly*, *36*, 72–80.

Wen, W., Cheng, S. Y., Chen, X. F., Wang, G., Li, S., Wang, X. Q., & Liu, X. Y. (2016). Impact of emission control on $PM_{2.5}$ and the chemical composition change in Beijing-Tianjin-Hebei during the APEC summit 2014. *Environmental Science and Pollution Research*, *23*(5), 4509–4521. https://doi.org/10.1007/s11356-015-5379-5

Whitaker, J. S., & Hamill, T. M. (2002). Ensemble data assimilation without perturbed observations. *Monthly Weather Review*, *130*(7), 1913–1924. https://doi.org/10.1175/1520-0493(2002)130%3C1913:Edawpo%3E2.0.Co;2

Xing, J., Zhang, Y., Wang, S., Liu, X., Cheng, S., Zhang, Q., et al. (2011). Modeling study on the air quality impacts from emission reductions and atypical meteorological conditions during the 2008 Beijing Olympics. *Atmospheric Environment*, *45*(10), 1786–1798. https://doi.org/10.1016/j.atmosenv.2011.01.025

Xu, W., Song, W., Zhang, Y., Liu, X., Zhang, L., Zhao, Y., et al. (2017). Air quality improvement in a megacity: Implications from 2015 Beijing parade blue pollution control actions. *Atmospheric Chemistry and Physics*, *17*(1), 31–46. https://doi.org/10.5194/acp-17-31-2017

Xue, Y., Wang, Y., Li, X., Tian, H., Nie, L., Wu, X., et al. (2017). Multi-dimension apportionment of clean air "parade blue" phenomenon in Beijing. *Journal of Environmental Sciences*, *65*, 29–42. https://doi.org/10.1016/j.jes.2017.03.035

Yang, W., Li, J., Zhu, L., & Wang, Z. (2013). Comparison of anthropogenic emission inventories of China mainland. *Research of Environmental Sciences*, *26*(7), 703–711.

Yumimoto, K., Uno, I., Sugimoto, N., Shimizu, A., Liu, Z., & Winker, D. M. (2008). Adjoint inversion modeling of Asian dust emission using lidar observations. *Atmospheric Chemistry and Physics*, *8*(11), 2869–2884. https://doi.org/10.5194/acp-8-2869-2008

Yumimoto, K., Uno, I., Sugimoto, N., Shimizu, A., & Satake, S. (2007). Adjoint inverse modeling of dust emission and transport over East Asia. *Geophysical Research Letters*, *34*, L08806. https://doi.org/10.1029/2006GL028551

Zhang, L., Shao, J. Y., Lu, X., Zhao, Y. H., Hu, Y. Y., Henze, D. K., et al. (2016). Sources and processes affecting fine particulate matter pollution over North China: An adjoint analysis of the Beijing APEC period. *Environmental Science & Technology*, *50*(16), 8731–8740. https://doi.org/10.1021/acs.est.6b03010

Zhang, Q., Streets, D. G., Carmichael, G. R., He, K. B., Huo, H., Kannari, A., et al. (2009). Asian emissions in 2006 for the NASA INTEX-B mission. *Atmospheric Chemistry and Physics*, *9*(14), 5131–5153. https://doi.org/10.5194/acp-9-5131-2009

Zhao, J., du, W., Zhang, Y., Wang, Q., Chen, C., Xu, W., et al. (2017). Insights into aerosol chemistry during the 2015 China Victory Day parade: Results from simultaneous measurements at ground level and 260 m in Beijing. *Atmospheric Chemistry and Physics*, *17*(4), 3215–3232. https://doi.org/10.5194/acp-17-3215-2017

Zhou, Y., Cheng, S. Y., Liu, L., & Chen, D. S. (2012). A coupled MM5-CMAQ modeling system for assessing effects of restriction measures on PM_{10} pollution in Olympic City of Beijing, China. *Journal Environmental Informatics*, *19*(2), 120–127. https://doi.org/10.3808/jei.201200214

Zhu, L., Henze, D. K., Cady-Pereira, K. E., Shephard, M. W., Luo, M., Pinder, R. W., et al. (2013). Constraining U.S. ammonia emissions using TES remote sensing observations and the GEOS-Chem adjoint model. *Journal of Geophysical Research: Atmospheres*, *118*, 3355–3368. https://doi.org/10.1002/jgrd.50166